Numerical Analysis of Tip Vortex Flow

Abolfazl Asnaghi, Andreas Feymark, Rickard E Bensow,
Chalmers University of Technology, Gothenburg/Sweden,
{abolfazl.asnaghi,andreas.feymark,rickard.bensow}@chalmers.se

The roll-up and formation of the tip vortex occur on the tip of a lifting wing of finite span. Close to the tip, a pressure differential exists between the upper and lower surfaces which drives the fluid around the tip from the high pressure side on the lower surface to the low pressure side on the upper surface. The fluid becomes highly three-dimensional as it undergoes this motion. The vortex then moves downstream and rolls up more and more of the wing wake until its circulation is nominally equal to that of the wing. This typically extends to a few wing spans downstream of the trailing edge. This proves to be a challenging flow field to study because of the presence of turbulence and the large gradients of pressure and velocity in all three directions especially across the vortex core.

In cavitation research and propeller design, tip vortex characteristics have a direct impact on the tip vortex cavitation inception which itself is important in defining the boundaries of the cavitation free bucket chart of a propeller. Due to the interaction of two phase flow and tip vortex, this phenomenon concerns very small scale dynamics making it very complicated to be studied through experimental or numerical tools. Understanding the physics of these flows therefore is important in finding the tip vortex inception speed in order to prevent or control the occurrence of cavitation on propellers.

Experimental analysis of tip vortex flow around elliptical foils have been performed by many researchers [1-4]. This type of foil has similar tip vortex behaviour as to a propeller making it a suitable benchmark for both numerical and experimental investigations of tip vortex flows.

In the experiments conducted by Arndt et al. [1-3], cavitation inception is studied on a series of elliptical planform hydrofoils, named Arndt elliptical foil. It is observed that the cavitation inception and its growth in the tip region strongly depends on the size and number of nuclei in the free stream and also on the strength of the vortex. Further, in most of the tested conditions the lowest pressure region of the tip vortex appears in a region very close to the tip where the vortex is not completely rolled up. It is also noted that for this type of foil, an excess axial velocity exists in the vortex core which increases with angle of attack; the axial velocity at the vortex core can go up to 2.4 times of the free stream velocity value. It is highlighted that the presence of bubbles in the flow and their trapping into the vortex does not significantly affect the vortex trajectory. The vortex is asymmetric, indicating the velocity measurements made with a single traverse through the vortex can be misleading. It is suggested to use particle image velocimetry (PIV) for further study and analysis. Observation indicates that the cavitation inception occurs both inside and outside the vortex core. Nuclei which cavitate just outside the core quickly spiral into the vortex axis. Moreover, it is noted that in strong water, where the amount of the nuclei is limited, larger bubbles are created when inception occurs. Then considering the inception pressure provides more consistent cavitation data than considering the saturation pressure. In the weak water it is found that the cavitation inception pressure was often greater than the saturation pressure. Moreover, significant level of tension can be tolerated before inception occurs in the strong water.

Following the suggestion by Arndt et al. [1-3] to use PIV method for tip vortex analysis, Pennings et al. [4] conducted Stereoscopic PIV measurements on the Arndt's foil in non-cavitating and cavitating conditions. They employed correlation averaging in PIV images post processing in order to minimize the interrogation area size.

The current paper reports parts of some tip vortex inception research undergoing in the Rolls-Royce University Technology Centre at Chalmers [5,6]. As a first step, numerical analysis of the wetted tip vortex around the Arndt elliptical foil is conducted using OpenFOAM.

The OpenFOAM package, used in this study for numerical simulation, is an open source code written in C++ to model and simulate fluid dynamics and continuum mechanics. It is possible to adopt the code and build new functionalities, libraries, solvers, and utilities. The software is community driven where various communities are working on different fields of applications. This has expedited the progress and development of the software. In OpenFOAM, the spatial discretization is performed using a cell centred collocated finite volume (FV) method for unstructured meshes with arbitrary cell

shapes, and a multi-step scheme is used for the time derivatives. To complete the FV-discretization the face fluxes need to be reconstructed from grid variables at adjacent cells, requiring interpolation of the convective fluxes and difference approximations for the inner derivatives of the diffusive fluxes; see [7-9] for more details on the discretization and the numerical schemes used in OpenFOAM.
The geometry of the Arndt foil is an elliptical planform having the NACA $66_2 - 145$ as cross section, see Figure 1. Having NACA 6 series section introduces a low adverse pressure gradient over the foil and therefore longer laminar boundary layer. The computational domain has the same dimensions and geometry as the cavitation tunnel at TU Delft. In Figure 2, the computational domain and related boundary positions are presented.

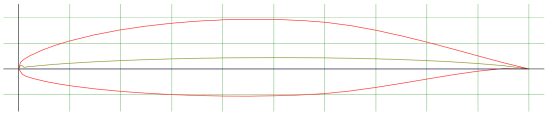

Figure 1. NACA $66_2 - 145$

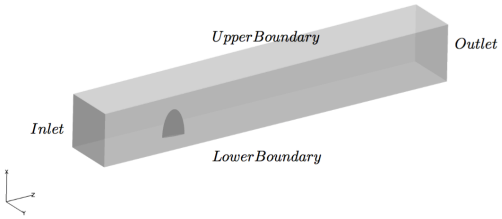

Figure 2. Boundary positions, Arndt foil

In the computational domain, the inlet is placed approximately five chord lengths in front of the foil, and the outlet is placed ten chord lengths behind the foil. The foil is positioned in the middle of the channel width where the distance to each side is equal to 150mm. The chord length of the foil at the root is equal to 125.6mm, and the coordinate system is located at the center of the chord. The trailing edge has been cut off with a thickness of 0.3mm, and the total area of the foil from the 3D CAD model is 0.01465 m^2. It should be noted that the current study is performed for the foil having geometrical angle of attack of 9 degrees. The inlet velocity is set equal to 6.8 m/s which corresponds to the Reynolds number of 8.5e05. The outlet pressure is set fixed equivalent to cavitation number four.
One of the most challenging parts of numerical analysis of tip vortex flows is to provide appropriate mesh resolution at the vortex core region. As one of the main tasks of the research was to find the spatial resolution requirement for numerical analysis of tip vortex flows, applying hexahedral cells at the tip vortex region became advantageous. To address this, StarCCM+ of CD-Adapco is used to generate the mesh.
At the first step, a coarse mesh is employed to simulate the tip vortex in order to find the approximate trajectory vortex path. The trajectory location is then used in StarCCM+ to define refinement zones. Two cylindrical regions are considered around the trajectory path to specify the mesh resolution, having 10 and 60 mm diameter, respectively, corresponding to approximately 10 and 60 times the vortex core diameter. These cylindrical regions extend two chord length downstream of the foil. In Figure 3 and 4, general distribution of the cells in the streamwise and inplane directions are presented.

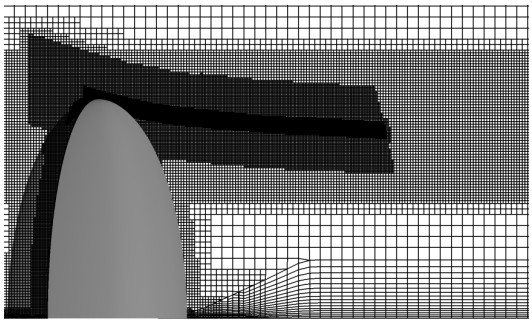

Figure 3. Streamwise mesh distribution

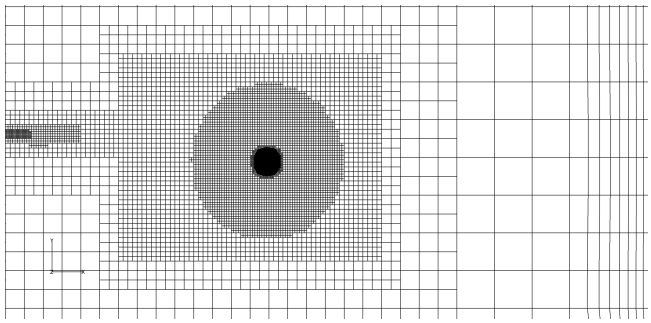

Figure 4. Inplane mesh distribution

Five different resolutions having different inplane and streamwise resolutions are created. The surface resolutions and prismatic layers (y^+=1) of these meshes are the same, and the only difference between them is the resolution of the inner refinement cylinder, Figure 4. In Table 1, the specifications of these

meshes are presented. It is reported that the tip vortex core for the selected operating condition has a diameter equal to 1 mm. Therefore, the sizes and dimensions in Table 1 are selected accordingly.

Table 1. Mesh specifications for mesh independency study

	Name	Total number of Cells (M)	In-plane cell size (mm)	Streamwise cell size (mm)	Number of cells in vortex core
In-Plane resolution	P1S1	8.3	0.125	0.25	8
	P2S1	24.4	0.062	0.25	16
	P3S1	88.3	0.031	0.25	32
Streamwise resolution	P2S1	24.4	0.062	0.25	16
	P2S2	44.3	0.062	0.125	16
	P2S3	84.9	0.062	0.062	16

Due to the computational resources limitation, the simulations are carried out in steady manner. The governing equations of a steady incompressible Newtonian fluid consist of conservation of mass, and momentum. In the filtered manner, these equations can be written as follow,

$$\frac{\partial(\overline{u_k})}{\partial x_k} = 0, \tag{1}$$

$$\frac{\partial(\overline{u_k}\,\overline{u_j})}{\partial x_j} = -\frac{1}{\rho}\frac{\partial \overline{p}}{\partial x_k} + \frac{\partial}{\partial x_j}\left[(\nu + \nu_t)\,\partial u_k/\partial x_j\right]. \tag{2}$$

To model the turbulent viscosity, the simulations are carried out as laminar (i.e. no turbulence model applied) and with kOmegaSST-RANS method [10]. The linear eddy viscosity assumption is insensitive to the flow streamline curvature, thus for highly swirling flows, this can lead to over prediction of turbulent viscosity in the swirling region. In order to compensate for that, various curvature corrections have been proposed [11].
For the kOmegaSST model, the empirical function that multiplies the production term P in both the k and ω equations is,

$$f_{r1} = max[min\{f_{rotation}, 1.25\}, 0], \tag{3}$$

where

$$f_{rotation} = (1 + C_{r1})\frac{2r^*}{1+r^*}[1 - C_{r3}tan^{-1}(C_{r2}\hat{r})] - C_{r1}. \tag{4}$$

All the variables and their derivatives are defined with respect to the reference frame of the calculation, which may be rotating with rotation rate Ω^{rot}. The remaining functions are defined as,

$$r^* = \frac{S}{W}, \tag{5}$$

$$\hat{r} = \frac{2W_{ih}S_{jh}}{WD^3}\left(\frac{DS_{ij}}{Dt} + \left(\varepsilon_{imn}S_{jn} + \varepsilon_{jmn}S_{in}\right)\Omega_m^{rot}\right), \tag{6}$$

$$S_{ij} = \frac{1}{2}\left(\frac{\partial u_i}{\partial x_j} + \frac{\partial u_j}{\partial x_i}\right), \tag{7}$$

$$W_{ij} = \frac{1}{2}\left[\left(\frac{\partial u_i}{\partial x_j} - \frac{\partial u_j}{\partial x_i}\right) + 2\varepsilon_{mji}\Omega_m^{rot}\right], \tag{8}$$

$$S^2 = 2S_{ij}S_{ij}, \tag{9}$$

$$W^2 = 2W_{ij}W_{ij}, \tag{10}$$

$$D^2 = max(S^2, 0.09W^2), \tag{11}$$

$$C_{r1} = 1.0,\ C_{r2} = 2.0,\ C_{r3} = 1.0. \quad (12)$$

The term DS_{ij}/Dt represents the components of the material derivative of the strain rate tensor. The rotation rate, Ω^{rot}, is nonzero only if the reference frame itself is rotating.
In Table 2, lift coefficient predictions using different mesh resolutions are presented. For laminar simulations, these different mesh resolutions show similar accuracy level in prediction of lift force (under predicted around 8 percent). The kωSST and kωSST-CC show over prediction of the lift force but in the same accuracy level. This indicates that the lift is unaffected by the prediction of the tip vortex. One reason for the difference between the laminar and the RANS results can be the effects of laminar-turbulent boundary layer transition. In the RANS simulation, the boundary layer is fully turbulent from the leading edge which contributes to the velocity distribution of the vortex core. To investigate further, one has to also model this case with a laminar-turbulent transitional RANS model.

Table 2. Lift coefficients for different mesh resolutions, laminar simulations

	In-plane refinement			Stream wise refinement			kωSST	kωSST-CC
Case	P1S1	P2S1	P3S1	P2S1	P2S2	P2S3	P2S1	P2S1
Lift Coefficient	0.604	0.605	0.608	0.605	0.605	0.606	0.716	0.714
Experiment	0.66							
Comparative Error %	-8.5	-8.3	-7.8	-8.3	-8.3	-8.2	8.5	8.2

Appearance of accelerated axial velocity at the vortex core decreases pressure below the saturation pressure. Therefore, in order to measure the distance that the vortex can be transported downstream, one can measure the length of the pressure iso-surface of $p=p_{sat}$. Figure 5 and Table 3 represent the iso-surface of pressure for different mesh resolution and also for different turbulence models. RANS simulations fail totally in predicting accelerated axial velocity, and as a result the length of the iso-surface is very short, just 12 mm. It should be also noted that no noticeable difference is observed by employing the curvature correction.

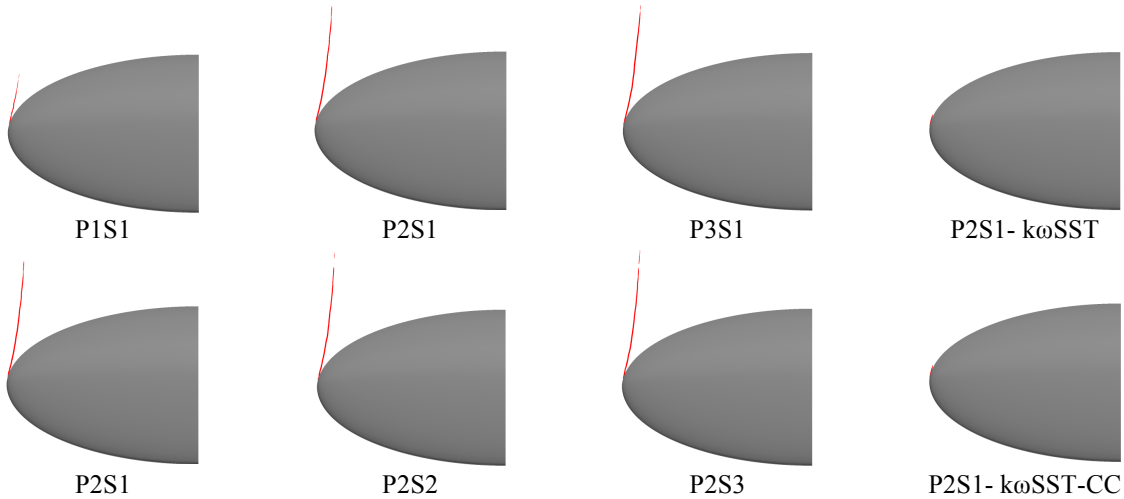

Figure 5. Pressure iso-surfaces ($p=p_{sat}$) for different mesh resolutions

Table 3. Pressure Iso-surface length ($p=p_{sat}$)

	In-plane refinement			Stream wise refinement			kωSST	kωSST-CC
Case	P1S1	P2S1	P3S1	P2S1	P2S2	P2S3	P2S1	P2S1
Length (mm)	43	96	98	96	107	107	12	12

For inplane resolution investigation, results of P2S1 is independent of the mesh resolution. Therefore, the cell size suggestion is 0.1 mm for inplane section which is equivalent to have 16 cells per vortex

core diameter. For streamwise resolution investigation, it is observed that for P2S2 mesh the convergence of results is achieved and results are independent of the resolution. Therefore, suggestion for the cell size in the streamwise direction is 0.2 mm corresponding to $1/8^{th}$ of the core diameter. For the cases that the vortex core diameter is not available, one can use Kolmogorov scale (η). For the current case, Kolmogorov scale was 5e-6 m. Therefore, the suggested sizes would be 20η for inplane resolution and 40η for streamwsie resolution.

Acknowledgements

Financial support of this work has been provided by Rolls-Royce Marine through the University Technology Centre in Computational Hydrodynamics hosted at the Dept. of Shipping and Marine Technology, Chalmers. The simulations were performed on resources at Chalmers Centre for Computational Science and Engineering (C3SE) provided by the Swedish National Infrastructure for Computing (SNIC).

References

[1] Arndt, Roger E.A.; Maines, Brant H. (1994). Viscous effects in tip vortex cavitation and nucleation. Retrieved from the University of Minnesota Digital Conservancy, http://purl.umn.edu/49809

[2] Arndt RA; Keller AP. Water Quality Effects on Cavitation Inception in a Trailing Vortex. ASME. *J. Fluids Eng.* 1992;114(3):430-438. doi:10.1115/1.2910049.

[3] R. E. A. Arndt, V. H. Arakeri and H. Higuchi (1991). Some observations of tip-vortex cavitation. Journal of Fluid Mechanics, 229, pp 269-289 doi:10.1017/S0022112091003026

[4] Pennings, P. C. and Westerweel, J. and van Terwisga, T. J. C., Flow field measurement around vortex cavitation, Experiments in Fluids, Vol 56, No 11, 2015.

[5] B. L. Zhang , J. Lou ; C. W. Kang ; A. Wilson ; J. Lundberg ; U. Svennberg ; Rickard E. Bensow; CFD Modeling of Propeller Tip Vortex over Large Distances; International Journal of Offshore and Polar Engineering (1053-5381). Vol. 24 (2014), 3, p. 181-183.

[6] Rickard E. Bensow, Mats G. Larson, Residual based VMS subgrid modeling for vortex flows, Computer Methods in Applied Mechanics and Engineering, Volume 199, Issues 13–16, 1 February 2010, Pages 802-809, ISSN 0045-7825, http://dx.doi.org/10.1016/j.cma.2009.08.004

[7] H. Jasak H.G. Weller, G. Tabor and C. Fureby, 'A tensorial approach to CFD using object oriented techniques'. Computational physics, 12, 1997.

[8] Hrvoje Jasak. 'Error Analysis and Estimation for the Finite Volume Method with Applications to Fluid Flows' PhD thesis, Department of Mechanical Engineering, Imperial College of Science, Technology and Medicine, 1996.

[9] Rusche Henrik. 'Computational Fluid Dynamics of Dispersed Two-Phase Flows at High Phase Fractions', PhD thesis, Department of Mechanical Engineering, University of London, Technology and Medicine, 2002.

[10] Gotfred S. Berntsen, Morten Kjeldsen, and Roger E. A. Arndt, Numerical modeling of sheet and tip vortex cavitation with fluent 5, CAV2001:sessionB5.006.

[11] Pavel E. Smirnov and Florian R. Menter, Sensitization of the SST Turbulence Model to Rotation and Curvature by Applying the Spalart–Shur Correction Term, Journal of Turbomachinery, OCTOBER 2009, Vol. 131